ADVANCED OPTICAL MATERIALS
www.advopticalmat.de

Solution-State Cooperative Luminescence Upconversion in Molecular Ytterbium Dimers

*Lohona K. Soro, Richard C. Knighton, Fernando Avecilla, Waygen Thor, Frédéric Przybilla, Olivier Jeannin, David Esteban-Gomez, Carlos Platas-Iglesias, and Loïc J. Charbonnière**

Two homometallic ytterbium dimers are prepared and their solution-state photoluminescence and upconversion properties are investigated. Both complexes exhibit two-photon cooperative luminescence upconversion in the visible region ($\lambda_{em} \approx 510$ nm) upon excitation into the near-infrared Yb $^2F_{5/2} \leftarrow {}^2F_{7/2}$ absorption band at 980 nm. This miniaturization of the cooperative luminescence phenomenon down to just two Yb ions unequivocally proves the mechanistic origins of this process. Time-resolved measurements and excited-state modeling indicate the presence of a slow recombination of two singly excited ions Yb*Yb* into a virtual excited state, which ultimately gives rise to the observed emission at ≈510 nm.

1. Introduction

Upconversion (UC), converse to conventional photoluminescence, is an anti-Stokes process whereby emission is generated via the piling up of multiple photons.[1] As a result of the anti-Stokes emission, UC is a process of choice for bio-analytical applications, removing spurious signals originating from autofluorescence of the samples and light scattering. Consequently, UC has found many applications such as in microscopy and photodynamic therapy,[2] remote cellular activation,[3] or bioassays.[4,5] However, these processes are typically observed in solid-state materials[6] or nanoparticles,[7] but a seminal example of energy transfer UC (ETU) at the molecular scale was reported by Piguet and co-workers in 2011, which consisted of a triply stranded Cr^{III}–Er^{III}–Cr^{III} helicate.[8,9] In the subsequent years this has been expanded to encompass a range of discrete upconverting systems, operating by excited state absorption (ESA),[10–12] energy transfer UC, or cooperative sensitizaton (CS).[15–18] At the molecular scale, much attention must be paid to minimize quenching due to the increased prevalence of nonradiative de-excitation processes from molecules in solution, primarily through OH, NH, and CH oscillators in the first or second coordination sphere.[20–22] This is achieved by using sterically encumbering ligand systems,[23] deuteration of the ligand scaffold,[16] or using perdeuterated solvents.[16,24,25]

One key impediment in the development of new molecular UC devices is the typical requirement to prepare heterometallic polyads, as is the case with CS systems comprising two or more Yb^{III} sensitizers around Tb^{III} or Ru^{II} acceptors (**Figure 1**a).[17,26] This approach, despite its effectiveness, is onerous due to the similar chemical reactivity between lanthanides,[27,28] as is the case for mixed Yb/Tb systems, which constrains the synthetic accessibility.[15,16]

Inspired by the pioneering work by Auzel[29] on solid-state materials,[30,31] we reported the first example of solution-state molecular cooperative luminescence (CL) using a Yb_9 cluster.[32] This entails double excitation of two proximate Yb^{III} ions at 980 nm which produces emission from a virtual excited state at 503 nm via a two-photon process (Figure 1b). While it is a key tenet of UC processes that the efficiency of UC is improved using more donor ions, there also remains the possibility of concentration quenching, which has been observed in nanoparticles.[33,34] Furthermore, the two-photon power dependence of the UC observed in homo-nonanuclear Yb_9 clusters supports the accepted mechanism of the requirement of only two proximate Yb^{III} ions. Conclusive confirmation of this dinuclear mechanism can only occur through removal of the extraneous Yb^{III} donors to its fundamental form in a dimeric Yb_2 system (*lex parsimoniae*). This strategy is not feasible in either

L. K. Soro, R. C. Knighton, W. Thor, L. J. Charbonnière
Equipe de Synthèse Pour l'Analyse (SynPA)
Institut Pluridisciplinaire Hubert Curien (IPHC)
UMR 7178
CNRS
Université de Strasbourg
ECPM, 25 rue Becquerel, Strasbourg Cedex 67087, France
E-mail: l.charbonn@unistra.fr
F. Avecilla, D. Esteban-Gomez, C. Platas-Iglesias
Centro de Investigacións Científicas Avanzadas (CICA) and
Departamento de Química
Universidade da Coruña
Campus da Zapateira-Rúa da Fraga 10, A Coruña 15008, Spain
F. Przybilla
Laboratoire de Bioimagerie et Pathologies
Faculté de Pharmacie CS60024 74
CNRS UMR 7021
Université de Strasbourg
Route du Rhin, Illkirch-Graffenstaden 67401, France
O. Jeannin
CNRS
ISCR-UMR 6226
Université de Rennes
Rennes F-35000, France
The ORCID identification number(s) for the author(s) of this article can be found under https://doi.org/10.1002/adom.202202307.

DOI: 10.1002/adom.202202307

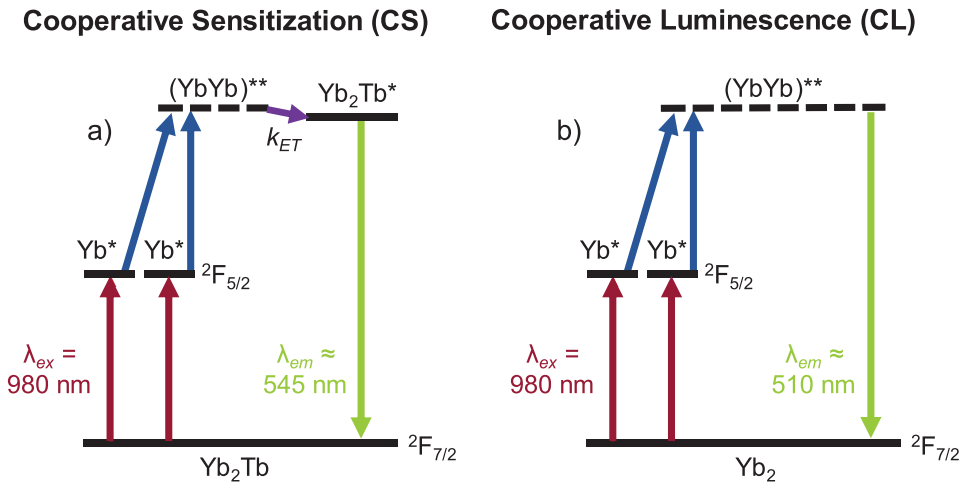

Figure 1. Energy transfer UC processes: a) CS in Yb_2Tb polynuclear species and b) CL in Yb_2 dimers.

solid-state or nanoparticular UC but is uniquely possible using a discrete molecular approach. As such we envisaged a miniaturization of the solution-state CL phenomenon down to its mechanistically simplest components using homo-dinuclear Yb_2 complexes, based upon both cryptate and tetra-imine bridging ligands.

2. Results and Discussion

The synthesis (**Scheme 1**) of the tricationic $[Yb_2L_1(NO_3)_2](NO_3)$ complex, following reported procedures,[35,36] consisted of a one-pot cyclization and complexation between tris(2-aminoethyl)amine (*tren*) and triethylammonium 2,6-diformyl-4-methylphenolate in the presence of $Yb(NO_3)_3$ to obtain the homo-dimetallic carciplex in 25% yield. The synthesis of the neutral bipyrimidine-bridged dimer was achieved by combination of $[Yb(ttfa)_3(OH_2)_2]$[37] (*ttfa* = thenoyltrifluoroacetylacetonate) and 2,2′-bipyrimidine (L_2) in anhydrous CH_3CN to obtain $[L_2(Yb(ttfa)_3)_2]$ in 45% yield as a microcrystalline solid. All complexes were characterised by NMR spectroscopy, mass spectrometry, and elemental analysis (Figures S1–S7, Supporting Information).

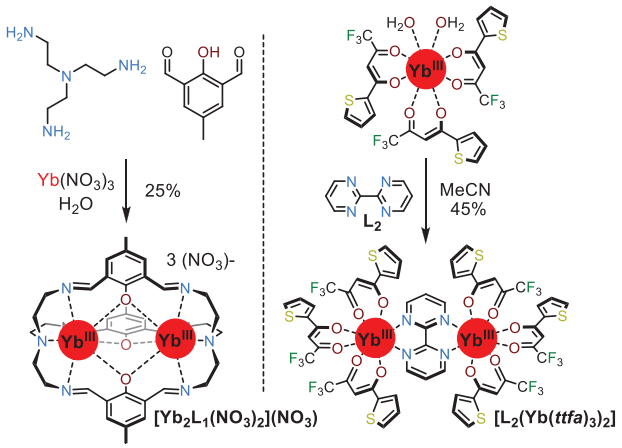

Scheme 1. Synthesis of Yb dimers used in this study.

Single crystals of $[Yb_2L_1(NO_3)_2](NO_3)$ and $[L_2(Yb(ttfa)_3)_2]$ suitable for single-crystal X-ray diffraction (SCXRD) analysis were obtained from slow evaporation of EtOH and CH_3CN solutions respectively. The coordination geometry of Yb^{III} for both complexes was initially investigated using the SHAPE 2.1 software using continuous shape measurement (CShM) (**Table 1**).[38] This software gives an indication of the metal center geometry where 0.000 corresponds to perfect polyhedron, i.e., a number closer to zero indicates a best fit for a given polyhedron. For the $[Yb_2L_1(NO_3)_2](NO_3)$ complex the geometry is best described as an octacoordinated triangular dodecahedron (TDD; Yb1 = 1.718, Yb2 = 1.964) but also resembles an octacoordinate biaugmented trigonal prism (BTPR; Yb1 = 2.311, Yb2 = 1.702). The two Yb^{III} centers are crystallographically nonequivalent and thus have different geometries in the solid state; however, this is likely due to crystallographic packing effects. Corresponding ChSM analysis of the DFT optimized structure of $[Yb_2L_1(DMSO)_2]^{3+}$ (vide infra DFT results), show much more symmetric Yb ions that indicates a TDD structure in solution (Yb1 = 1.599, Yb2 = 1.580). For the $[L_2(Yb(ttfa)_3)_2]$ complex the geometry is clearly that of an eight-coordinate square antiprism (SAP) environment (Yb1 = 0.424), exhibiting minimal distortion, the heteroleptic coordination environment notwithstanding. This is again reflected in the DFT results (vide infra) for $L_2(Yb(ttfa)_3)_2]$ which confirms the SAP geometry (Yb1 = 0.415).

Analyzing the structure of $[Yb_2L_1(NO_3)_2](NO_3)$, the complex crystallizes in the $P4_12_12$ space group with solvent molecules in the unit cell, perpetuated by an H-bonding network with cocrystallized disordered H_2O which primarily interacts with the free and bound nitrate counterions (**Figure 2**; Table S1 and Figures S8 and S9, Supporting Information). Bond lengths and angles are summarized in Figure S10 and Tables S2 and S3 (Supporting Information). Both of the crystallographically distinct Yb ions are encapsulated in the trianionic cryptate cavity, although both display similar geometries at the Yb centers. They are each octacoordinated, bound to the bridgehead tertiary nitrogen and three flanking imine groups of the *tren* moiety.

Table 1. CShM analysis of the SCXRD and DFT structures of $[Yb_2L_1(NO_3)_2](NO_3)$ and $[L_2(Yb(ttfa)_3)_2]$.

Structure		SAP	TDD	BTPR
$[Yb_2L_1](NO_3)_3$ (XRD)	Yb1	2.536	1.718	2.311
	Yb2	2.240	1.964	1.702
$[Yb_2L_1(DMSO)_2]^{3+}$ (DFT)	Yb1	3.253	1.599	2.472
	Yb2	3.150	1.580	2.377
$[L_2(Yb(ttfa)_3)_2]$ (XRD)	Yb1	0.424	2.596	2.337
$[L_2(Yb(ttfa)_3)_2]$ (DFT)	Yb1	0.415	2.450	1.864

The bridgehead nitrogen displays relatively elongated distance (d(Yb–N_{amine} (mean)) = 2.64 Å) compared to the imine donors (d(Yb–N_{imine} (mean)) = 2.40 Å), arising from the geometric constraints of the ligand. The two metal centers display an internuclear distance of 3.4450(3) Å and are linked via three μ_2-phenolate groups (d(Yb–$O_{phenolate}$ (mean)) = 2.32 Å). The metal ions sit at the apical and basal vertices of a highly symmetrical trigonal bipyramid, the equatorial sites comprising the three oxygen donors, with a high degree of linearity compared to the phenolate centroid (∡Yb1–$Cnt_{phenolate}$–Yb2 = 176.67(14)°; d(Yb1–$Cnt_{phenolate}$) = 1.721(2)Å, d(Yb2–$Cnt_{phenolate}$) = 1.726(2)Å) . The final eighth coordination site is occupied by an oxygen atom of a nitrate counterion (d(Yb–$O_{nitrate}$ (mean)) = 2.35 Å). A second oxygen atom provides a weak interaction with Yb1 (Yb1–O8 = 2.993(5) Å). The compound is enantiopure in the solid state; the ligand overall exhibits chirality imparted to helical twisting of the phenolate moieties to satisfy the metal coordination, while each half displays a *syn*-rotatory helicity at the metal center[35,36] (i.e., Δ,Δ arrangements with Flack parameter = 0.016(12)).

SCXRD analysis of $[L_2(Yb(ttfa)_3)_2]$ (**Figure 3**; Table S4 and Figures S11 and S12, Supporting Information) reveals that the complex crystallizes in the orthorhombic $P2_1/n$ space group, displaying a plane of symmetry through the central 2,2′-bipyrimidine ligand with one ytterbium ion in the asymmetric unit. The internuclear lanthanide Yb1–Yb1 distance was found to be 6.639 Å, with only a slight deviation from the mean plane defined by the 2,2′-bipyrimidine (Yb1–Pln_{bpm} = 0.220 Å; Figure S13, Supporting Information). The Yb ions are eight-coordinated (Figure S14 and Table S5, Supporting Information), satisfied by three anionic *ttfa* ligands corresponding to six oxygen donors (Mean distance Yb–O_{ttfa} = 2.26 Å), with the coordination sphere completed by two nitrogen donors from the bridging 2,2′-bipyridimine ligand (Mean distance Yb–N_{bpm} = 2.52 Å). Aside from the heteroleptic donor environment around the Yb ion, the geometry is consistent with a slightly distorted square antiprism (SAP–D_{4d}) with average skew angles (φ) of 45.03° between the upper and lower square faces, which are separated by 2.532(2) Å. Other metrics which can be analyzed are the structure geometry versus an ideal square anti-prism. Figure 3c,d shows the sides formed by the upper and lower square faces of the SAP polyhedron (d_{in}) as well as the distance between the two mean square faces (d_{pp}(Pln–Pln)). d_{pp} is only slightly perturbed from parallel (∡Pln–Pln = 1.54(9)°). Other salient observations are the d_{pp}(Pln–Pln) distance (2.53 Å), which is shorter than the average internuclear distance (d_{in}) between the atoms lying on the vertices of the square faces (Mean value of d_{in} = 2.75 Å), while $d_{pp} = d_{in}$ in a perfect SAP geometry. Likewise, the average calculated value of α of 57.06° is more open compared to the perfect SAP (α_{ideal} = 54.73°).[39,40] Both these observations indicate that the geometry at Yb exhibits a splaying and compression versus the ideal geometry.

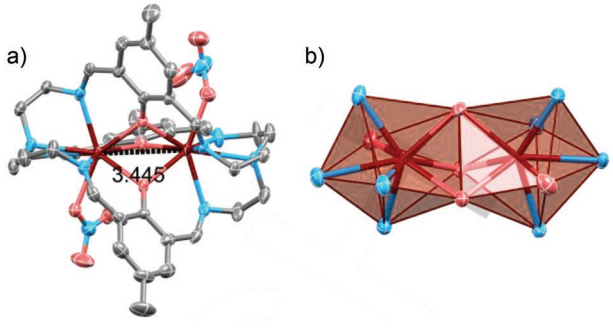

Figure 2. Single-crystal X-ray structure of $[Yb_2L_1(NO_3)_2](NO_3)$ (ellipsoids are plotted at the 50% probability level, and H atoms, non-coordinating anions, and disorder are omitted for clarity, CCDC 2203544): a) full structure and b) polyhedral view of the Yb_2 coordination environment.

The absorption, excitation and luminescence spectra of $[Yb_2L_1(NO_3)_2](NO_3)$ in DMSO are presented in **Figure 4**, with the main spectroscopic data gathered in **Table 2**. The UV–vis absorption spectrum displays a strong absorption band (maximum at λ = 370 nm, ε = 20200 M^{-1} cm^{-1}) attributed to the $\pi^* \leftarrow \pi$ transitions of the coordinated bis-iminophenolate moieties. In the NIR domain, weak Stark-split Yb^{III} $^2F_{5/2} \leftarrow {}^2F_{7/2}$ absorption bands are observed between 900 and 1050 nm (maximum at λ = 977 nm, ε = 13.3 M^{-1} cm^{-1}). The downshifted emission spectra of the complex upon ligand excitation induces Yb^{III}-centered $^2F_{5/2} \rightarrow {}^2F_{7/2}$ emission bands with maxima at 977 nm, with weaker lower energy bands at 1006 and 1030 nm. Time resolved studies measured on the main emission band of $[Yb_2L_1(NO_3)_2](NO_3)$ revealed a biexponential decay with lifetimes of 8.3 µs (83%) and 18.7 µs (17%), likely a result of a combination of DMSO and NO_3^- ligands competing for the 8th coordination site not satisfied by ligand L_1.

From the NIR absorption spectra, the methodology of Werts and co-workers[41] was applied to determine the radiative lifetime of Yb in the complex using Equation (1) and (2)

$$\frac{1}{\tau_{rad}} = 2303 \times \frac{8\pi c n^2 \tilde{\nu}^2}{N_A} \frac{g_l}{g_u} \int \varepsilon(\tilde{\nu})\, d\tilde{\nu} \quad (1)$$

$$\tilde{\nu} = \frac{\int \tilde{\nu} \times \varepsilon(\tilde{\nu})\, d\tilde{\nu}}{\int \varepsilon(\tilde{\nu})\, d\tilde{\nu}} \quad (2)$$

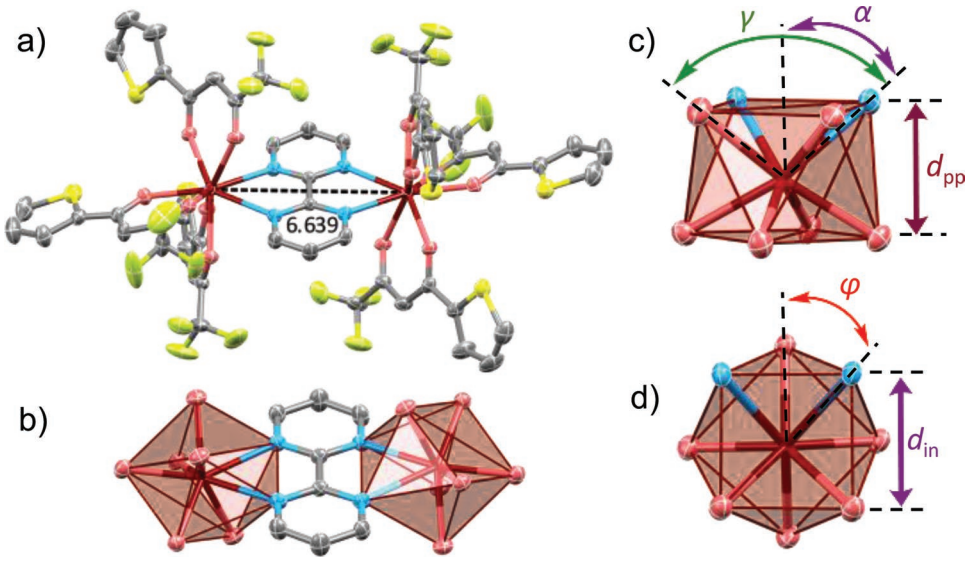

Figure 3. Single-crystal X-ray structure of $[L_2(Yb(ttfa)_3)_2]$ (ellipsoids are plotted at the 50% probability level, and H atoms and disorder are omitted for clarity, CCDC 2209638): a) full structure, b) polyhedral view of the Yb_2 coordination environment, c) polyhedral view of Yb environment, and d) view along the pseudo-S_8 axis.

In which N_A is Avogadro's number, $\tilde{\upsilon}$ is the barycenter of the transition (cm^{-1}), c is the speed of light in vacuum (cm s^{-1}), n is the refractive index of the solvent, $\varepsilon(\tilde{\upsilon})$ is the absorption spectrum of the transition (M^{-1} cm^{-1}).

Weighted by the number of Yb centers (divided by 2 in comparison to the values reported in Table 2), g_l and g_u are related to the degeneracies of the ground and excited states, respectively, and are equal to $2J + 1$ where $J = 7/2$ for g_l and $J = 5/2$ for g_u.

A radiative lifetime of 587 µs was determined for Yb in the $[Yb_2L_1(NO_3)_2](NO_3)$ complex. The Yb centered luminescence quantum yield, Φ_{Yb}^{Yb}, could then be calculated using Equation (3)

$$\Phi_{Yb}^{Yb} = \frac{\tau_{obs}}{\tau_{rad}} \quad (3)$$

Considering that the $[Yb_2L_1(NO_3)_2](NO_3)$ complex displayed a biexponential behavior, the intensity averaged luminescence decay lifetime[42] of 10.1 µs was used for the calculations. The Yb centered quantum yield was then calculated to be 0.017.

The fine structure of the absorption and downshifted photoluminescence (Figure 4a) indicates Stark-split sublevels of the $^2F_{7/2}$ and $^2F_{5/2}$ ground and excited states (Figure 4b), which was further investigated using CASSCF/NEVPT2/QDPT calculations. For the complex of L_1, calculations were performed on the $[Yb_2L_1(DMSO)_2]$ system, as the NO_3^- anions coordinated in the solid state are very likely replaced by DMSO ligands, as a result of their similar donor character and the large excess of DMSO present in solution.[43]

Results of the theoretical calculations are presented in **Table 3**. The three main emission bands as well as the shoulder at 1050 nm observed in the emission spectrum correspond to transitions between the lowest Stark level of the $^2F_{5/2}$ excited state to the Stark levels of the ground $^2F_{7/2}$ state. Thus, the main emission band at 977 nm matches with the calculated (4 → 0) transition, denoted A. This is borne out for the other emission bands at 1002 nm (4 → 1, transition B), 1024 nm (4 → 2, transition C), and 1050 nm (4 → 3, transition D). We note that the emission components at 1002 and 1024 nm match very well the weak (hot) absorptions observed on the low energy side of the absorption spectrum. The theoretical CASSCF/NEVPT2/QDPT calculations provide reasonably good agreement with the experimental data, which supports our assignment. Furthermore, calculations provided the highest oscillator strength for the (4 ← 0) transition calculated at ≈987 nm, which also contains further intensity contribution from the hot (5 ← 1) transition, in agreement with the experimental spectra.

The speciation of $[Ln(ttfa)_3)_2]$ complexes has been widely reported in the literature[46–51] and it is known that at very low concentrations complex mixtures can occur through dissociation of one or more of the ligands. Our study within reports these results with care and does not discount the possibility of some dissociation. However, the UC spectra reported are on relatively concentrated samples which minimize the potential for dissociation and we can conclude that the dimetallic species are the main species at these concentrations.

The absorption, excitation, and luminescence spectra of $[L_2(Yb(ttfa)_3)_2]$ in CH_3CN are presented in **Figure 5**, with the main spectroscopic data gathered in Table 2. The complex exhibits significantly more intense ligand-centered absorptions (λ = 336 nm, ε = 115 000 M^{-1} cm^{-1}), ascribable to an overlap of π^* ← π transitions on both the bridging μ_2-bpm ligand and six peripheral *ttfa* ligands.[52] Again, weak absorption bands corresponding to the absorption of the Yb^{III} $^2F_{5/2}$ ← $^2F_{7/2}$ transition was observed from ≈900 to 1050 nm (λ = 976 nm, ε = 11.6 M^{-1} cm^{-1}; Figure 5a). Correspondingly, $[L_2(Yb(ttfa)_3)_2]$ displays relatively more intense lower energy transitions at 1007 and 1030 nm. In contrast, the Yb excited state lifetime of the $[L_2(Yb(ttfa)_3)_2]$ complex was found to be monoexponential at 18.3 µs. A radiative lifetime of 710 µs was obtained (Equation (1)), resulting in a Yb centered luminescence quantum yield of 0.026. This value for $[L_2(Yb(ttfa)_3)_2]$ agrees with previously reported literature values for similar

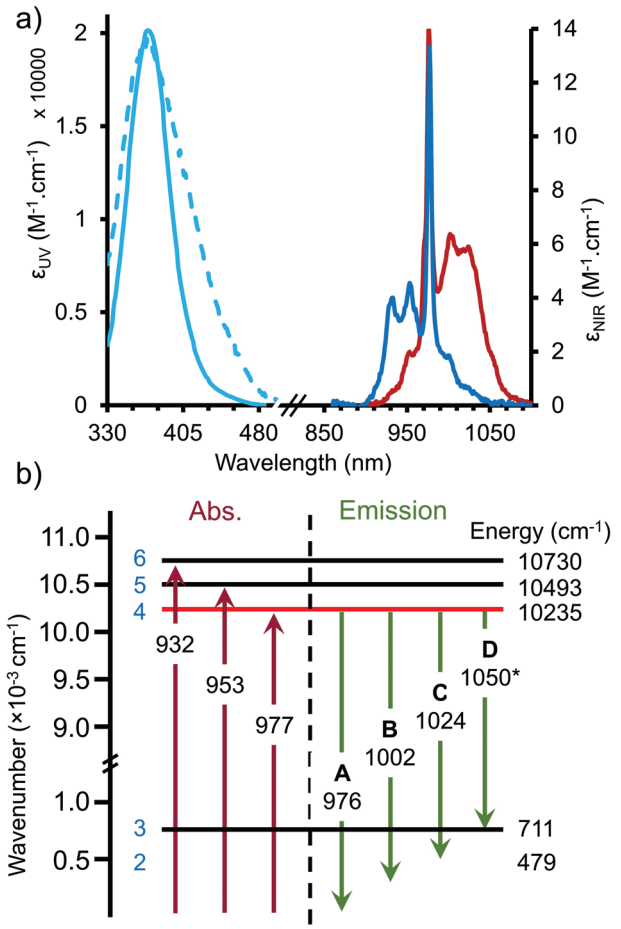

Figure 4. a) Absorption spectra in the UV (blue solid line, 1.15×10^{-5} M) and NIR (dark blue, 3.4×10^{-3} M) ranges and normalized excitation (blue dashed lines, $\lambda_{em} = 980$ nm) and emission (red line, $\lambda_{ex} = 370$ nm) spectra of the $[Yb_2L_1(NO_3)_2](NO_3)$ complex in DMSO. b) Energy level diagram for $[Yb_2L_1(NO_3)_2](NO_3)$. Each horizontal line represents a Kramer's doublet.

compounds containing Yb(*ttfa*)$_3$ fragments (0.0046–0.042).[53,54] For $[L_2(Yb(ttfa)_3)_2]$ (Figure 5b), the three main emission bands are observed at 976 nm (4 → 0, transition A), 1005 nm (4 → 1, transition B) and 1032 nm (4 → 2, transition C). Despite the observation of emission beyond 1050 nm, the fourth transition (4 → 3, transition D) could not be resolved on our setup experimentally, although the 4 ← 3 energy gap was determined computationally to be 1044 nm (**Table 4**). The 4 ← 3 transition is characterized by a very low oscillator strength according to CASSCF/NEVPT2/QDPT calculations.

Following the elucidation of the downshifted photoluminescent properties of the two complexes, UC experiments were undertaken (**Figure 6**). Direct excitation into the Yb $^2F_{5/2} \leftarrow {}^2F_{7/2}$ absorption bands (λ_{ex} = 980 nm) gave rise to upconverted emission in the visible region with maxima at 502 and 512 nm, respectively, for $[Yb_2L_1(NO_3)_2](NO_3)$ in DMSO-d_6 and $[L_2(Yb(ttfa)_3)_2]$ in CH_3CN, with a large anti-Stokes shift (>9400 cm^{-1}).

The two-photon behavior of the UC emission was confirmed using Log/Log plots (Figure 6b,e), showing a quadratic dependence of the incident laser intensity. The calculated slopes of the Log/Log plots, 1.93 and 1.66, respectively, for $[Yb_2L_1(NO_3)_2](NO_3)$ and $[L_2(Yb(ttfa)_3)_2]$, were indeed close to the theoretical value of two, indicating that it operates through a two-photon process consistent with the phenomenon of CL. One notable observation is the respective maxima of the UC emission. $[L_2(Yb(ttfa)_3)_2]$ (λ_{UC} = 512 nm) displays a 10 nm bathochromic shift with respect to $[Yb_2L_1(NO_3)_2](NO_3)$ (λ_{UC} = 502 nm), which can be understood by the increased prevalence of the low energy emission bands (B and C; Figures 4b and 5b) and thus a bigger contribution from the two-photon lower-energy transitions.[55]

Considering that CL arises from the relaxation of two transitions on two distinct Yb excited ions, the intensity $F(\lambda)$ of the CL at wavelength λ is the result of all possible combinations between these levels and can be calculated by a convolution of the NIR emission spectrum $f(\nu l)$ (Equation (4); Section S5.1 and Figures S16 and S17, Supporting Information)[29,56,57]

$$F(\lambda) = \int f(\lambda') f(\lambda - \lambda') d\lambda' \quad (4)$$

The convoluted spectra can be found in Figure 6a,d, respectively, for $[Yb_2L_1(NO_3)_2](NO_3)$ and $[L_2(Yb(ttfa)_3)_2]$. The maxima of the calculated CL emissions are found at 513.0 and 516.5 nm, respectively, in rather good agreement with the observed maxima in the measured spectra (resp. 502 and 512). As anticipated, the maximum for $[L_2(Yb(ttfa)_3)_2]$ is bathochromically shifted, as a result of the larger contributions from the more intense band at low energy observed in the emission spectrum of $[L_2(Yb(ttfa)_3)_2]$ (Figure 5) compared to that of $[Yb_2L_1(NO_3)_2](NO_3)$ (Figure 4).

The UC quantum yield (UCQY) of dinuclear $[Yb_2L_1(NO_3)_2](NO_3)$ was determined to be 47×10^{-9} which compares favorably with our previous nonanuclear CL system, $[Yb_9(OD)_{10}(acac)_{16}]^+$ which has a UCQY of 3.0×10^{-9}.[29] The UCQY of $[L_2(Yb(ttfa)_3)_2]$ in CH_3CN was determined to be 0.23×10^{-9}, which increased to 6.9×10^{-9} in CD_3CN. This smaller value can be explained by the much lower downshifted emission quantum yield, and the increased Yb–Yb distance of 6.639 Å (cf. 3.445 Å for $[Yb_2L_1(NO_3)_2](NO_3)$). However, both complexes confirm that CL can occur in systems with only two proximate Yb ions and with comparable efficiencies as those containing a much higher local concentration of potential donors.

Finally, we investigated the evolution of the UC signal using time-resolved measurements in which the sample is excited during 100 µs irradiation with a repetition rate of 50 kHz (**Figure 7**c,f). During the excitation period, the UC signal develops to reach a quasi-steady state within ≈30 µs. When the excitation is switch off, the UC CL decays rapidly after the pulse. The energy-level diagram in Figure 7 shows the excited-state process occurring to engender upconverted CL, inspired by the mechanism proposed by Güdel et al. for weakly coupled dimers generating CS.[58] Firstly a single Yb^{III} ion is excited (k_{exc}) to form Yb*Yb, which subsequently absorbs another photon to form a Yb*Yb* doubly excited state. This is proceeded by a slow recombination step (k_{UC}) to form a doubly excited (YbYb)** ion pair which then emits in the visible region with a corresponding lifetime $\tau_{Yb^{**}}$.

Considering the rise and decay of the luminescence intensity of the (YbYb)** CL of the Yb dimers, the populations of the

Table 2. Photophysical properties of the different complexes obtained in DMSO for $[Yb_2L_1(NO_3)_2](NO_3)$ and CH_3CN for $[L_2(Yb(ttfa)_3)_2]$.

	ε_{Ligand} [M^{-1} cm^{-1}] (λ [nm])	ε_{Yb} [M^{-1} cm^{-1}] (λ [nm])	τ_{Yb} [µs][a)]	τ_{radYb} [µs]	$\Phi_{Yb}^{Lb)}$ [%]	Φ_{Yb} [%]	η_{sens} [%]	Φ_{UC}[d)] [% × 10^{-7}]
$[Yb_2L_1(NO_3)_2](NO_3)$	20 200 (370)	13.3 (977)	8.3 (83%) 18.7 (17%)	587	1.0	1.7[c)]	57	47[e)]
$L_2(Yb(ttfa)_3)_2$	45 200 (266) 115 000 (336)	11.6 (976)	18.3	710	0.04	2.6	1.6	0.23 6.9[f)]

[a)]Excitation at 370 nm for $[Yb_2L_1](NO_3)_3$ and 336 for $[L_2(Yb(ttfa)_3)_2]$; [b)]Using cardiogreen (IR125) in MeOH ($\Phi = 0.078$; $\lambda_{exc} = 765$ nm) as reference[44]; [c)]Calculated using an intensity average lifetime; [d)]Excitation at 980 nm in DMSO-d_6, CH_3CN, or CD_3CN ($P = 6.9$ W cm^{-2}), using Rhodamine6G in water ($\Phi = 0.76$; $\lambda_{exc} = 488$ nm) as reference[45] for the UC quantum yield, and errors estimated at 15%; [e)]Value obtained in DMSO-d_6; [f)]Obtained in CD_3CN.

different states, denoted as $|0\rangle$ to $|3\rangle$ (Figure 7) can be modeled with the following matrix

$$\begin{pmatrix} |0\rangle \\ |1\rangle \\ |2\rangle \\ |3\rangle \end{pmatrix} = \begin{pmatrix} -2k_{exc} & k_{Yb^*} & 0 & k_{Yb^{**}} \\ 2k_{exc} & -k_{Yb^*} - k_{exc} & 2k_{Yb^*} & 0 \\ 0 & k_{exc} & -2k_{Yb^*} - k_{UC} & 0 \\ 0 & 0 & k_{UC} & -k_{Yb^{**}} \end{pmatrix} \times \begin{pmatrix} |0\rangle \\ |1\rangle \\ |2\rangle \\ |3\rangle \end{pmatrix} \quad (5)$$

where k_{exc}, the pumping rate constant can be defined as

$$k_{exc} = \frac{\lambda_p}{hc} P\sigma_{Yb}^{0\to1} \quad (6)$$

where λ_p is the excitation wavelength (980 nm), h is Planck's constant, c is the vacuum speed of light, P is the incident pump intensity and $\sigma_{Yb}^{0\to1}$ is the absorption cross section (in cm^2 per molecule) of the Yb $^2F_{7/2} \rightarrow {}^2F_{5/2}$ transition obtained from the electronic absorption spectrum. In the case of $[Yb_2L_1(NO_3)_2](NO_3)$, the decay rate of Yb, k_{Yb^*} is fixed at 0.099×10^6 s^{-1} (averaged lifetime of 10.1 µs). $k_{Yb^{**}}$ is the decay rate of the CL from (YbYb)** and k_{UC} is the energy transfer from Yb*Yb* to (YbYb)**. The temporal evolution of the (YbYb)** was fitted according to the proposed model in two steps, first fitting the rise of the signal ($k_{exc} \neq 0$), then fitting the decay ($k_{exc} = 0$) keeping other parameters as constants to the rise in the fitting. The luminescence intensity is assumed to be proportional to the population of state $|3\rangle$. Full experimental details about the fitting procedure are given in the Supporting Information (Section S5.2, Supporting Information).

With this mathematical model, the best fitting curve yields the values of k_{UC} and $k_{Yb^{**}}$ as $18.03 \pm 0.05 \times 10^6$ s^{-1} and $0.74 \pm 0.03 \times 10^6$ s^{-1}, respectively. It is worth noting that the rate

Table 3. Absorption spectral data obtained with CASSCF/NEVPT2/QDPT calculations and experimental data obtained from absorption and emission spectroscopy for complex $[Yb_2L_1(NO_3)_2](NO_3)$.

Transition[a)] (pop.)[b)]	λ [nm]	Energy [cm^{-1}]	$10^9 \times f_{osc}$	Exp [nm][c)]	Exp [nm][d)]
4 ↔ 0 (0.634)	986.7	10 134.9	420	977	977
5 ↔ 0 (0.634)	963.8	10 375.9	184	953	
6 ↔ 0 (0.634)	948.0	10 548.0	148	932	
4 ↔ 1 (0.204)	1010.3	9898.4	78	1000	1002
5 ↔ 1 (0.204)	986.3	10 139.3	120		
6 ↔ 1 (0.204)	969.8	10 311.5	40		
4 ↔ 2 (0.105)	1024.6	9759.6	16	1024	1024
5 ↔ 2 (0.105)	999.9	10 000.6	38		
6 ↔ 2 (0.105)	983.0	10 172.8	24		
4 ↔ 3 (0.058)	1037.5	9639.0	8		1050
5 ↔ 3 (0.058)	1012.1	9880.0	10		
6 ↔ 3 (0.058)	994.8	10 052.1	4		

[a)]Calculations were performed on the $[Yb_2L_1(DMSO)_2]^{3+}$ system, see text; [b)]Boltzmann populations of the lowest energy level involved in the transition at 300 K provided within parentheses; [c)]Data from absorption spectra; [d)]Data from emission spectra.

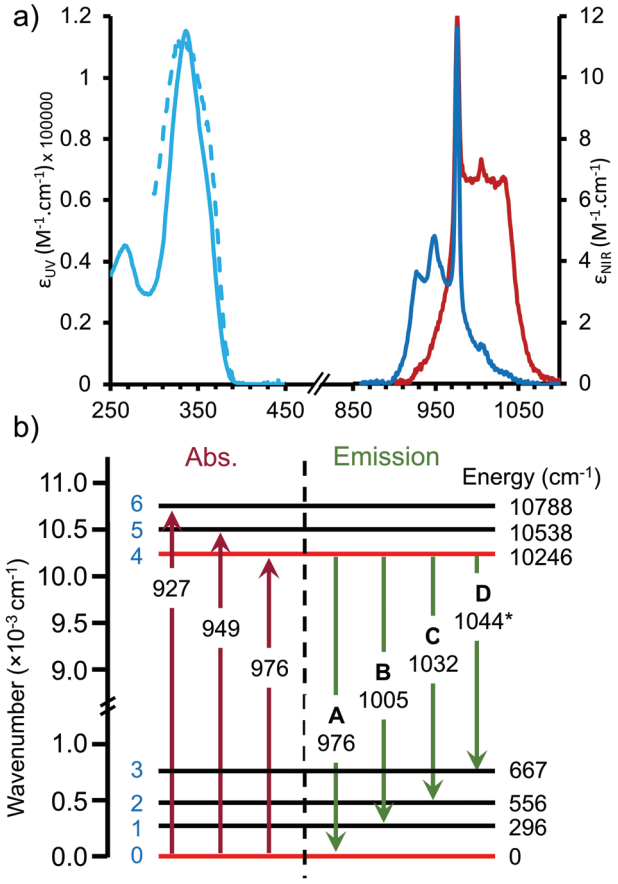

Figure 5. a) Absorption spectra in the UV (blue solid line, 5.75×10^{-6} M) and NIR (dark blue, 4.4×10^{-3} M) ranges and normalized excitation (blue dashed lines, $\lambda_{em} = 980$ nm) and emission (red line, $\lambda_{ex} = 336$ nm) spectra of the $[L_2(Yb(ttfa)_3)_2]$ complex in CH_3CN. b) Energy diagram for $[L_2(Yb(ttfa)_3)_2]$, where each horizontal line represents a Kramer's doublet (* denotes a transition determined computationally).

Table 4. Absorption spectral data obtained with CASSCF/NEVPT2/QDPT calculations and experimental data obtained from absorption and emission spectroscopy for complex $[L_2(Yb(ttfa)_3)_2]$.

Transition (pop.)[a]	λ [nm]	Energy [cm^{-1}]	$10^9 \times f_{osc}$	Exp [nm][b]	Exp [nm][c]
4 ← 0 (0.634)	985.6	10 146.0	446	976	976
5 ← 0 (0.634)	966.6	10 345.9	440	949	
6 ← 0 (0.634)	943.4	10 599.6	182	927	
4 ← 1 (0.196)	1010.0	9901.1	74	1005	1005
5 ← 1 (0.196)	990.0	10 101.0	38		
6 ← 1 (0.196)	965.7	10 354.7	24		
4 ← 2 (0.128)	1019.1	9812.2	42		1032
5 ← 2 (0.128)	998.8	10 012.1	44		
6 ← 2 (0.128)	974.1	10 265.8	14		
4 ← 3 (0.042)	1044.0	9578.8	4		
5 ← 3 (0.042)	1022.6	9778.6	10		
6 ← 3 (0.042)	996.8	10 032.4	2		

[a]Boltzmann populations of the lowest energy level involved in the transition at 300 K provided within parentheses; [b]Data from absorption spectra; [c]Data from emission spectra.

of $k_{Yb^{**}}$ (corresponding to a lifetime $\tau_{Yb^{**}} = 1/k_{Yb^{**}} = 1.4$ µs) is faster than expected according to previous reports assuming it to be twice the rate of de-excitation of Yb*,[55] but such a phenomenon has already been observed for solid state CL.[29] When fixing the value of $k_{Yb^{**}}$ to $2k_{Yb^{*}}$, the fitting process failed to adjust the experiment time-resolved luminescence spectra (Figure S18, Supporting Information). On the other hand, changing the k_{UC} changes the decay behaviour of the Yb** luminescence, implying the key role of k_{UC} in the CL (Figure S19, Supporting Information).

Similarly, k_{UC} and $k_{Yb^{**}}$ could be obtained for the case of $[L_2(Yb(ttfa)_3)_2]$ using $k_{Yb^{*}} = 0.055$ (Yb* lifetime of 18.3 µs). Values of $k_{UC} = 18.84 \pm 0.01 \times 10^6$ s^{-1} and $k_{Yb^{**}} = 0.19 \pm 0.05 \times 10^6$ s^{-1} were determined. Here again, the excited state lifetime obtained for $\tau_{Yb^{**}} = 1/k_{Yb^{**}} = 5.1$ µs, is shorter than expected ($\tau_{Yb^{**}theo} = \tau_{Yb^{*}}/2 = 9.1$ µs), but to a lesser extent than for the $[Yb_2L_1(NO_3)_2](NO_3)$ analog. Among the possible explanations of this shortening, an energy back transfer from Yb** to the ligand centered triplet state, might be envisaged. In both cases, the energy transfer rate constants leading

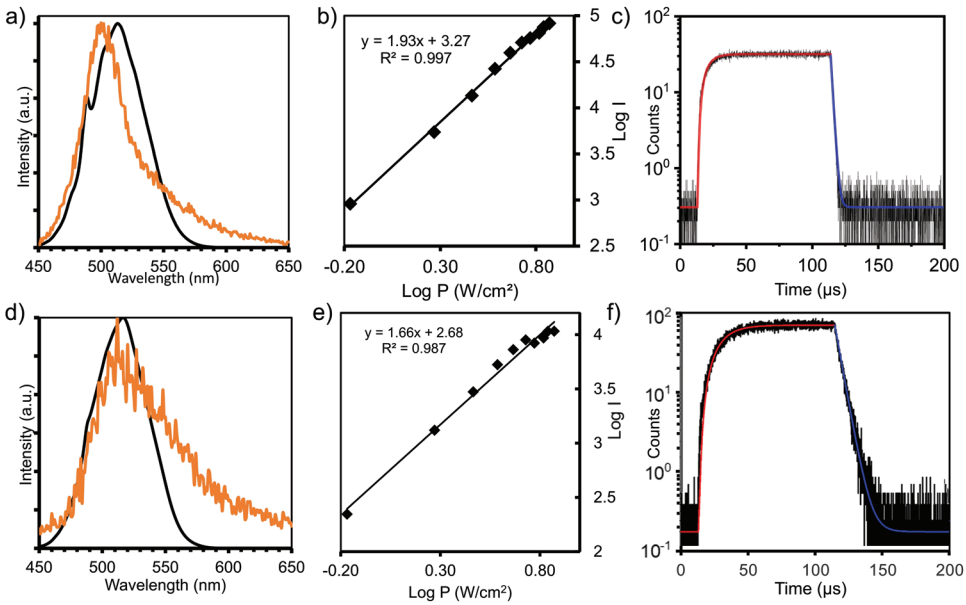

Figure 6. a) UC emission of $[Yb_2L_1(NO_3)_2](NO_3)$ in DMSO ($[3.25 \times 10^{-3}$ M], $\lambda_{exc} = 980$ nm, $P = 6.9$ W cm^{-2}, NS = 10) and d) of $[L_2(Yb(ttfa)_3)_2]$ ($[3.70 \times 10^{-3}$ M] in CH_3CN, $\lambda_{exc} = 980$ nm, $P = 6.9$ W cm^{-2}, NS = 20) (experimental UC spectra represented by an orange line, convoluted spectra represented by black line). b) UC intensity as a function of the incident pump power density of $[Yb_2L_1(NO_3)_2](NO_3)$ in DMSO (3.25×10^{-3} M) and e) of $[L_2(Yb(ttfa)_3)_2]$ (3.70×10^{-3} M) in CH_3CN. c) Time-resolved rise and decay curves of the UC emission at 510 ± 10 nm upon time-gated excitation at 974 nm (8.1 kW cm^{-2} (black line)) of $[Yb_2L_1(NO_3)_2](NO_3)$ in DMSO and f) of $[L_2(Yb(ttfa)_3)_2]$ in CH_3CN. The red and blue lines correspond to the fit of the rise and decay respectively (see text).

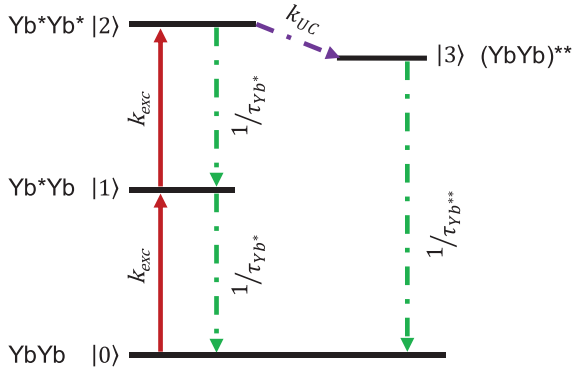

Figure 7. Energy level diagram of the CL UC mechanism in the Yb dimers.

to the UC process, k_{UC}, are faster than the rate of de-excitation of Yb*, allowing for the CL to take place. It is worth noting that the $k_{Yb^{**}}$ is faster in $[Yb_2L_1(NO_3)_2](NO_3)$ with the shorter intermetallic distance. Interestingly, despite the shorter intermetallic Yb distance in $[Yb_2L_1(NO_3)_2](NO_3)$ compared to $[L_2(Yb(ttfa)_3)_2]$, the energy transfer step is not found to be faster.

3. Conclusion

Two homo-dimetallic Yb complexes have been prepared, based upon a triphenolic cryptate and a bipyridine-bridged ttfa complex via operationally simple one-step protocols. Both complexes were crystallized and analysis by SCXRD displays intermetallic distances of 3.445 and 6.639 Å, respectively. The absorption and emission properties of the complexes were fully studied and photoluminescence experiments upon ligand excitation gave rise to Yb-centered emission in the NIR region (λ_{em} = 976 nm), for which theoretical calculations elucidated the Starks splitting of the $^2F_{5/2}$ and $^2F_{7/2}$ energy levels. Upon direct Yb excitation (λ_{ex} = 980 nm) CL could be observed in the visible region ($\lambda_{em} \approx$ 510 nm). The slight bathochromic shift observed in the CL spectrum of $[L_2(Yb(ttfa)_3)_2]$ compared to $[Yb_2L_1(NO_3)_2](NO_3)$ could be rationalized by convolution of the emission arising from the Yb centered $^2F_{5/2} \leftarrow {}^2F_{7/2}$ emission band. The observed CLQY were found to be still modest, but similar or better than nonanuclear complexes in solution.[32]

The CL was also analyzed using time-resolved spectroscopy and modeling of the excited state kinetics, revealing a slow UC energy-transfer step from an intermediate Yb*Yb* state which converts to a doubly excited state (YbYb)**, which is ultimately responsible for the CL emission. Although slow, the energy transfer rate for UC appeared faster than the direct de-excitation of Yb*, allowing the UC to occur. Possible improvements of CL in Yb dimers may be found in the further development of very long lived Yb complexes.[59] This molecular approach using only two Yb ions allows us unique insight into probing this enigmatic CL process, fully confirming the purported mechanism. The factors affecting the CLQY appear to be complicated but clearly determinants for efficient UC performance are related to the intermetallic distance and the lifetime of the double excited state (Yb**). Future rational design for improving the QY would focus on reducing this intermetallic distance and reducing nonradiative quenching pathways. One significant contribution is the potential of Yb to Yb energy transfer deactivation which results—perhaps unexpectedly—in improved UCQY for molecular dimers versus Yb_9 clusters.

Supporting Information

Supporting Information is available from the Wiley Online Library or from the author.

Acknowledgements

Financial support is gratefully acknowledged (L.J.C. and R.C.K.) from the French Ministère de l'Education Nationale et de la Recherche, the French Canada Research Fund (L.K.S.), Frontier Research in Chemistry Foundation (LabEx CSC, ANR-10-LABX-0026_CSC), and the French National research agency (LAPIN project no. ANR-20-CE09-0021-02; LUCAS project no. ANR-19-CE29-0014-01). C.P.-I. thanks the Centro de Computación de Galicia (CESGA) for providing the computer facilities and the Ministerio de Ciencia e Innovación (Grant PID2019-104626GB-I00). Benjamin Beaufils is thanked for the synthesis of 2,2′-bipyrimidine.

Conflict of Interest

The authors declare no conflict of interest.

Data Availability Statement

The data that support the findings of this study are available in the supplementary material of this article.

Keywords

cooperative luminescence, lanthanides, photoluminescence, upconversion

Received: September 30, 2022
Revised: November 28, 2022
Published online: December 22, 2022

[1] F. Auzel, *J. Lumin.* **1990**, *45*, 341.
[2] X. Zhang, F. Ai, T. Sun, F. Wang, G. Zhu, *Inorg. Chem.* **2016**, *55*, 3872.
[3] X. Ai, L. Lyu, Y. Zhang, Y. Tang, J. Mu, F. Liu, Y. Zhou, Z. Zuo, G. Liu, B. Xing, *Angew. Chem., Int. Ed.* **2017**, *56*, 3031.
[4] G. Huang, Y. Zhu, S. Wen, H. Mei, Y. Liu, D. Wang, M. Maddahfar, Q. P. Su, G. Lin, Y. Chen, D. Jin, *Nano Lett.* **2022**, *22*, 3761.
[5] L. Mattsson, K. D. Wegner, N. Hildebrandt, T. Soukka, *RSC Adv.* **2015**, *5*, 13270.
[6] Y. Shi, M. Yuan, J. Li, F. Li, W. Cui, X. Jiao, Y. Peng, Y. Huang, L. Chen, *Inorg. Chem.* **2022**, *13*, 5309.
[7] S. Wen, J. Zhou, K. Zheng, A. Bednarkiewicz, X. Liu, D. Jin, *Nat. Commun.* **2018**, *9*, 2415.
[8] L. Aboshyan-Sorgho, C. Besnard, P. Pattison, K. R. Kittilstved, A. Aebischer, J.-C. G. Bünzli, A. Hauser, C. Piguet, *Angew. Chem., Int. Ed.* **2011**, *50*, 4108.

[9] L. Aboshyan-Sorgho, M. Cantuel, S. Petoud, A. Hauser, C. Piguet, *Coord. Chem. Rev.* **2012**, *256*, 1644.
[10] A. Nonat, C. F. Chan, T. Liu, C. Platas-Iglesias, Z. Liu, W.-T. Wong, W.-K. Wong, K.-L. Wong, L. J. Charbonnière, *Nat. Commun.* **2016**, *7*, 11978.
[11] O. A. Blackburn, M. Tropiano, T. J. Sørensen, J. Thom, A. Beeby, L. M. Bushby, D. Parker, L. S. Natrajan, S. Faulkner, *Phys. Chem. Chem. Phys.* **2012**, *14*, 13378.
[12] J. H. S. K. Monteiro, E. A. Hiti, E. E. Hardy, G. R. Wilkinson, J. D. Gorden, A. E. V. Gorden, A. de Bettencourt-Dias, *Chem. Commun.* **2021**, *57*, 2551.
[13] D. A. Gálico, J. S. Ovens, F. A. Sigoli, M. Murugesu, *ACS Nano* **2021**, *15*, 5580.
[14] B. Golesorkhi, S. Naseri, L. Guénée, I. Taarit, F. Alves, H. Nozary, C. Piguet, *J. Am. Chem. Soc.* **2021**, *143*, 15326.
[15] J. Wang, Y. Jiang, J.-Y. Liu, H.-B. Xu, Y.-X. Zhang, X. Peng, M. Kurmoo, S. W. Ng, M.-H. Zeng, *Angew. Chem., Int. Ed.* **2021**, *60*, 22368.
[16] N. Souri, P. Tian, C. Platas-Iglesias, K.-L. Wong, A. Nonat, L. J. Charbonnière, *J. Am. Chem. Soc.* **2017**, *139*, 1456.
[17] A. Nonat, S. Bahamyirou, A. Lecointre, F. Przybilla, Y. Mély, C. Platas-Iglesias, F. Camerel, O. Jeannin, L. J. Charbonnière, *J. Am. Chem. Soc.* **2019**, *141*, 1568.
[18] L. K. Soro, C. Charpentier, F. Przybilla, Y. Mély, A. M. Nonat, L. J. Charbonnière, *Chemistry* **2021**, *3*, 1037.
[19] D. A. Gálico, R. Ramdani, M. Murugesu, *Nanoscale* **2022**, *14*, 9675.
[20] A. M. Nonat, L. J. Charbonnière, *Coord. Chem. Rev.* **2020**, *409*, 213192.
[21] W. D. Horrocks, D. R. Sudnick, *J. Am. Chem. Soc.* **1979**, *101*, 334.
[22] A. Beeby, I. M. Clarkson, R. S. Dickins, S. Faulkner, D. Parker, L. Royle, A. S. de Sousa, J. A. Gareth Williams, M. Woods, *J. Chem. Soc. Perkin Trans.* **1999**, *2*, 493.
[23] H. Bolvin, A. Fürstenberg, B. Golesorkhi, H. Nozary, I. Taarit, C. Piguet, *Acc. Chem. Res.* **2022**, *55*, 442.
[24] I. Hyppänen, S. Lahtinen, T. Ääritalo, J. Mäkelä, J. Kankare, T. Soukka, *ACS Photonics* **2014**, *1*, 394.
[25] R. C. Knighton, L. K. Soro, A. Lecointre, G. Pilet, A. Fateeva, L. Pontille, L. Francés-Soriano, N. Hildebrandt, L. J. Charbonnière, *Chem. Commun.* **2021**, *57*, 53.
[26] R. C. Knighton, L. K. Soro, W. Thor, J.-M. Strub, S. Cianférani, Y. Mély, M. Lenertz, K.-L. Wong, C. Platas-Iglesias, F. Przybilla, L. J. Charbonnière, *J. Am. Chem. Soc.* **2022**, *144*, 13356.
[27] X.-Z. Li, L.-P. Zhou, L.-L. Yan, Y.-M. Dong, Z.-L. Bai, X.-Q. Sun, J. Diwu, S. Wang, J.-C. Bünzli, Q.-F. Sun, *Nat. Commun.* **2018**, *9*, 547.
[28] T. J. Sørensen, S. Faulkner, *Acc. Chem. Res.* **2018**, *51*, 2493.
[29] B. Schaudel, P. Goldner, M. Prassas, F. Auzel, *J. Alloys Compd.* **2000**, *300-301*, 443.
[30] S. Magne, Y. Ouerdane, M. Druetta, J. P. Goure, P. Ferdinand, G. Monnom, *Opt. Commun.* **1994**, *111*, 310.
[31] X. Chen, S. Li, Z. Song, W. Du, O. Wen, N. Sawanobori, *J. Opt. Soc. Am. B* **2006**, *23*, 2581.
[32] R. C. Knighton, L. K. Soro, L. Francés-Soriano, A. Rodríguez-Rodríguez, G. Pilet, M. Lenertz, C. Platas-Iglesias, N. Hildebrandt, L. J. Charbonnière, *Angew. Chem., Int. Ed.* **2022**, *61*, e202113114.
[33] B. Chen, F. Wang, *Acc. Chem. Res.* **2020**, *53*, 358.
[34] H. Dong, L.-D. Sun, C.-H. Yan, *Chem. Soc. Rev.* **2015**, *44*, 1608.
[35] C. Platas, F. Avecilla, A. de Blas, T. Rodríguez-Blas, C. F. G. C. Geraldes, É. Tóth, A. E. Merbach, J.-C. G. Bünzli, *J. Chem. Soc. Dalton Trans.* **2000**, *4*, 611.
[36] F. Avecilla, A. de Blas, C. Platas, T. Rodríguez-Blas, R. Bastida, A. Macías, A. Rodríguez, D. E. Fenton, J. Mahía, *Chem. Commun.* **1999**, *2*, 125.
[37] P. Lenaerts, K. Driesen, R. Van Deun, K. Binnemans, *Chem. Mater.* **2005**, *17*, 2148.
[38] D. Casanova, M. Llunell, P. Alemany, S. Alvarez, *Chemistry* **2005**, *11*, 1479.
[39] H.-S. Wang, K. Zhang, J. Wang, Z. Hu, Y. Song, Z. Zhang, Z.-Q. Pan, *CrystEngComm* **2021**, *23*, 3175.
[40] S. Alvarez, P. Alemany, D. Casanova, J. Cirera, M. Llunell, D. Avnir, *Coord. Chem. Rev.* **2005**, *249*, 1693.
[41] M. H. V. Werts, R. T. F. Jukes, J. W. Verhoeven, *Phys. Chem. Chem. Phys.* **2002**, *4*, 1542.
[42] M. N. Berberan Santos, B. Valeur, *Molecular Fluorescence: Principles and Applications*, 2nd ed., **2012**.
[43] R. Díaz-Torres, S. Alvarez, *Dalton Trans.* **2011**, *40*, 10742.
[44] R. C. Benson, H. A. Kues, *Phys. Med. Biol.* **1978**, *23*, 159.
[45] J. Olmsted, *J. Phys. Chem.* **1979**, *83*, 2581.
[46] D. Y. Chappidi, M. N. Gordon, H. M. Ashberry, J. Huang, B. M. Labedis, R. E. Cooper, B. J. Cooper, V. Carta, S. E. Skrabalak, K. R. Dunbar, E. M. Fatila, *Inorg. Chem.* **2022**, *61*, 12197.
[47] L. Fioravanti, L. Bellucci, L. Armelao, G. Bottaro, F. Marchetti, F. Pineider, G. Poneti, S. Samaritani, L. Labella, *Inorg. Chem.* **2022**, *61*, 265.
[48] A. Zaïm, H. Nozary, L. Guénée, C. Besnard, J.-F. Lemonnier, S. Petoud, C. Piguet, *Chemistry* **2012**, *18*, 7155.
[49] A. Zaïm, N. D. Favera, L. Guénée, H. Nozary, T. N. Y. Hoang, S. V. Eliseeva, S. Petoud, C. Piguet, *Chem. Sci.* **2013**, *4*, 1125.
[50] L. Babel, T. N. Y. Hoang, H. Nozary, J. Salamanca, L. Guénée, C. Piguet, *Inorg. Chem.* **2014**, *53*, 3568.
[51] K. Baudet, V. Kale, M. Mirzakhani, L. Babel, S. Naseri, C. Besnard, H. Nozary, C. Piguet, *Inorg. Chem.* **2020**, *59*, 62.
[52] P. Kadjane, L. Charbonnière, F. Camerel, P. P. Lainé, R. Ziessel, *J. Fluoresc.* **2008**, *18*, 119.
[53] N. M. Shavaleev, S. J. A. Pope, Z. R. Bell, S. Faulkner, M. D. Ward, *Dalton Trans.* **2003**, 808.
[54] B. Li, H. Li, P. Chen, W. Sun, C. Wang, T. Gao, P. Yan, *Phys. Chem. Chem. Phys.* **2015**, *17*, 30510.
[55] E. Nakazawa, S. Shionoya, *Phys. Rev. Lett.* **1970**, *25*, 1710.
[56] P. Goldner, F. Pellé, D. Meichenin, F. Auzel, *J. Lumin.* **1997**, *71*, 137.
[57] W. Qin, Z. Liu, C.-N. Sin, C. Wu, G. Qin, Z. Chen, K. Zheng, *Light Sci. Appl.* **2014**, *3*, e193.
[58] G. M. Salley, R. Valiente, H. U. Guedel, *J. Lumin.* **2001**, *94–95*, 305.
[59] Z. Zhu, G.-Q. Jin, J. Wu, X. Ying, C. Zhao, J.-L. Zhang, J. Tang, *Inorg. Chem. Front.* **2022**.